

Limitations of Charge Transfer State Parameterization Using Photovoltaic External Quantum Efficiency

Ardalan Armin,* Nasim Zarrabi, Oskar J. Sandberg, Christina Kaiser, Stefan Zeiske, Wei Li, and Paul Meredith*

Free carrier photogeneration in bulk-heterojunction solar cells composed of blends of acceptor and donor organic semiconductors proceeds via intermolecular charge transfer (CT) states. Non-adiabatic Marcus theory has proven valid to explain the absorption and emission of these sub-gap states which have extremely weak emission probabilities and absorption cross sections making them difficult to probe directly using optical spectroscopy. Therefore, the CT state parameters involved in the Marcus model are often extracted from fittings on the photovoltaic external quantum efficiency (EQE_{PV}) and electroluminescence. These two spectra are (ideally) interrelated via the so-called reciprocity principle. In this paper, the limitations of such an approach are demonstrated, in particular the impact of simple low finesse cavity interference effects acting as an uneven spectral filter for emission and absorption. This can produce almost spurious CT state parameterization with, for example, relative errors as large as 90% in absorption coefficients obtained from EQE_{PV} . It is shown how these limitations can be partially lifted using an iterative transfer matrix approach applied to the EQE_{PV} .

1. Introduction

Due to their relatively low dielectric constants, organic semiconductors are generally considered “excitonic materials” in which electrons and holes remain bound upon photoexcitation.^[1] Efficient charge generation in these systems can be achieved by the use of two semiconducting materials, namely a donor and acceptor with (often) different molecular orbital energies—that is to say electron affinities and ionization potentials. The energy offset between the highest occupied molecular orbital of the donor and the energy of the lowest unoccupied molecular orbital of the


acceptor in the so-called bulk-heterojunction (BHJ) organic solar cell results in new hybrid intermolecular charge transfer (CT) states^[2] which determine the effective band gap and thereby the open circuit voltage.^[3] These CT states mediate the charge photogeneration between the excitons and relaxed free charges, and thus their kinetics determine most of the recombination processes^[4,5] and the thermodynamic limit of the solar cell.^[3,6] The open circuit voltage of any solar cell is determined primarily by the band gap energy (i.e., the energy of the CT states in the case of BHJs), band-to-band recombination, and non-radiative recombination.^[7,8] These all add up to different contributions in the losses in the open circuit voltage (the loss being the difference between the energy gap and the observed open circuit voltage).^[9] The radiative limit of the open circuit voltage is governed by the solar photon absorption by the singlet exci-

tions and thermal photon absorption by the CT states, while non-radiative losses are related to how efficiently these states emit.^[8] Through the so-called reciprocity principle, the emission and absorption spectra are interrelated intrinsically, although for low mobility organic semiconductors with substantial second order recombination there may be deviations from this principle.^[10] Energetic disorder and non-equilibrium states can also play a role in deviations from this principle as shown recently.^[11] As such, if the CT states are fully characterized, the open circuit voltage can be explained or predicted to within some accuracy.^[8] The energy and dynamics of the CT states also contain quite profound information from a structure-property-design consideration. Thus, from multiple perspectives, CT state analysis has become a central theme in not just organic solar cells, but organic optoelectronics more broadly.^[12]

Inspired from models of partially radiative ion pairs, non-adiabatic Marcus theory has been employed to explain the thermal broadening of the CT states, their emission, and absorption.^[13,14] This parameterization includes an energy of the CT state (E_{CT}), reorganization energy (λ_{CT}), and oscillator strength (f_{σ}) related to the electronic coupling, as well as emission probability f_i . Ideally, the absorption cross-section (σ_{CT}) and emission (I) are related through reciprocity so that

$$\sigma_{CT} = \frac{f_{\sigma}}{E\sqrt{4\pi\lambda_{CT}k_B T}} \exp\left(-\frac{(E_{CT} + \lambda_{CT} - E)^2}{4\lambda_{CT}k_B T}\right) \quad (1)$$

Dr. A. Armin, N. Zarrabi, Dr. O. J. Sandberg, C. Kaiser, S. Zeiske, Dr. W. Li, Prof. P. Meredith
Sustainable Advanced Materials (Sêr SAM)
Department of Physics
Swansea University
Singleton Park, Swansea SA2 8PP, U.K.
E-mail: ardalan.armin@swansea.ac.uk; paul.meredith@swansea.ac.uk

 The ORCID identification number(s) for the author(s) of this article can be found under <https://doi.org/10.1002/aenm.202001828>.

© 2020 The Authors. Published by Wiley-VCH GmbH. This is an open access article under the terms of the Creative Commons Attribution License, which permits use, distribution and reproduction in any medium, provided the original work is properly cited.

DOI: 10.1002/aenm.202001828

$$I = \frac{f_I E}{\sqrt{4\pi\lambda_{CT}k_B T}} \exp\left(-\frac{(E_{CT} - \lambda_{CT} - E)^2}{4\lambda_{CT}k_B T}\right) \quad (2)$$

where k_B is the Boltzmann constant, T the absolute temperature, and E the photon energy. To determine these parameters, the absorption and/or emission of CT states must be accurately measured and fittings to Equations (1) and (2) performed. However, as CT states are weak dipoles, their contribution to the light absorption and their emission efficiency are likewise extremely weak—demanding very sensitive measurement techniques.

Sensitive emission spectrophotometry can be used to measure electroluminescence (EL) or photoluminescence (PL) spectra from which the energy of CT states and their reorganization energy can be obtained by fittings to Equation (2). However, List et al. have shown that the spectral shape of the EL spectrum is significantly influenced by thickness-dependent light out-coupling hence causing an apparent deviation from Equation (2).^[15] This deviation can be understood by considering organic solar cells as low finesse optical cavities acting as spectral filters and are thus subject to interference effects—the mode structure and coupling of which are thickness dependent. The CT parameters can also be obtained from fittings on the absorption spectra of the CT states if they are spectrally decoupled from the singlet excitons. To determine the light absorption due to the sub-gap states including CT states, photothermal deflection spectroscopy has been used^[16,17] as well as photocurrent-based techniques such as Fourier transform photocurrent spectroscopy^[18] and photovoltaic external quantum efficiency (EQE_{PV}).^[13] The latter can be measured extremely sensitively to determine the sub-gap absorption due to CT states and trap states (corrected for interference effects) as recently shown by the authors.^[19] While the CT state and reorganization energies can be potentially obtained from the EQE_{PV} spectral line-shape, the oscillator strength requires knowledge of the absorption coefficient (α) spectrum. From Equation (1) the absorption coefficient for CT states can be defined when the density of CT states (N_{CT}) is known:

$$\alpha_{CT} = \frac{f_\alpha}{E\sqrt{4\pi\lambda_{CT}k_B T}} \exp\left(-\frac{(E_{CT} + \lambda_{CT} - E)^2}{4\lambda_{CT}k_B T}\right) \quad (3)$$

where f_α (herein referred to as absorption pre-factor) is related to the oscillator strength via $f_\alpha = N_{CT}f_\sigma$. This spectrum is often inferred from the EQE_{PV} with the Beer–Lambert assumption in the low-absorbance limit^[7] so that

$$\text{Abs} \approx EQE_{PV} \approx 2d\alpha_{CT} \quad (4)$$

where d is the junction thickness and Abs is the absorbance of the active layer. A factor of 2 is sometimes included to account for the double pass due to the reflecting metallic electrode of the solar cell. The role of non-unity internal quantum efficiency can also be included in Equation (4) to rule out the losses due to recombination but assuming said losses to be energy independent. In essence, Equation (4) requires that the absorbance (and the EQE_{PV}) reflect the exact spectral shape of the absorption coefficient—which as we shall see is not always the case.

In this communication we expand upon the work of List et al. where they showed interference effects significantly impact the spectral shape of the EL and thus the obtained CT state parameters. These interference effects are known to influence the spectral shape of the EQE_{PV} above the optical-gap^[20,21] but their impact on the sub-gap region is largely ignored. We also demonstrate that the parameterization can be strongly affected by the optical interference when obtained from the EQE_{PV} —the extent to which is dependent on the material refractive indices, device structure, and junction thickness. This impact is mainly due to the invalidity of Equation (4) in the presence of reflective electrodes, and we present an analytical approximation which is useful in dealing with it. To exemplify these parameterization issues, we present an analysis of six different fullerene and non-fullerene acceptor (NFA) organic BHJ solar cells. We show that while apparently acceptable fittings can be obtained on EQE_{PV} and EL spectra, the extracted CT state and reorganization energies from EQE_{PV} and EL can be quite different. These limitations arise from how light absorption (in-coupling) and emission (out-coupling) are affected differently by the low-finesse cavity mode whose energy is dependent upon the thickness of the junction. This is probed and quantified in detail for one given system, and we specifically demonstrate that the absorption pre-factor (f_α) obtained from fittings on the absorption coefficient estimated from the EQE_{PV} via Equation (4) contains a large relative error which is thickness dependent. This questions the validity of Equation (4) even for order-of-magnitude estimations. To exclude any additional and unknown experimental issues such as measurement geometry, we then numerically simulate (dummy) EQE_{PV} and EL spectra using a full device model with known CT parameters, and attempt to recalculate these parameters using the same fitting procedure which was applied to the experimental results. In such a manner, we confirm that the error caused by device wave-optics on the extracted CT state parameters are significant and cannot be neglected. To overcome these complications in the fittings and to obtain correct CT parameters we utilize a recently introduced approach^[12,22] to extract the absorption coefficient (thickness independent and absent of interference) by an inverse iterative transfer matrix method from the EQE_{PV} spectra. This approach appears to-date the most accurate method to parameterize the CT states for their energy, reorganization energy, and absorption pre-factor based upon the EQE_{PV} and is complementary to that recently presented by List et al. based upon EL spectra. It is also important to emphasize that we do not claim any fundamental violation of the detailed balance principle, merely that the apparent reciprocity represented by Equations (1) and (2) is broken by interference effects. The degree of this deviation from reciprocity—caused essentially by the cavity acting as an uneven spectral filter—is dependent upon the cavity thickness, quality-factor, refractive indices of all layers, and emission/absorption wavelengths and corresponding Stokes shift.

2. Results

To exemplify the accuracy of the fittings and CT analysis based upon Equations (1) and (2) on EQE_{PV} and EL spectra we selected six different BHJ solar cell material combinations. The chemical

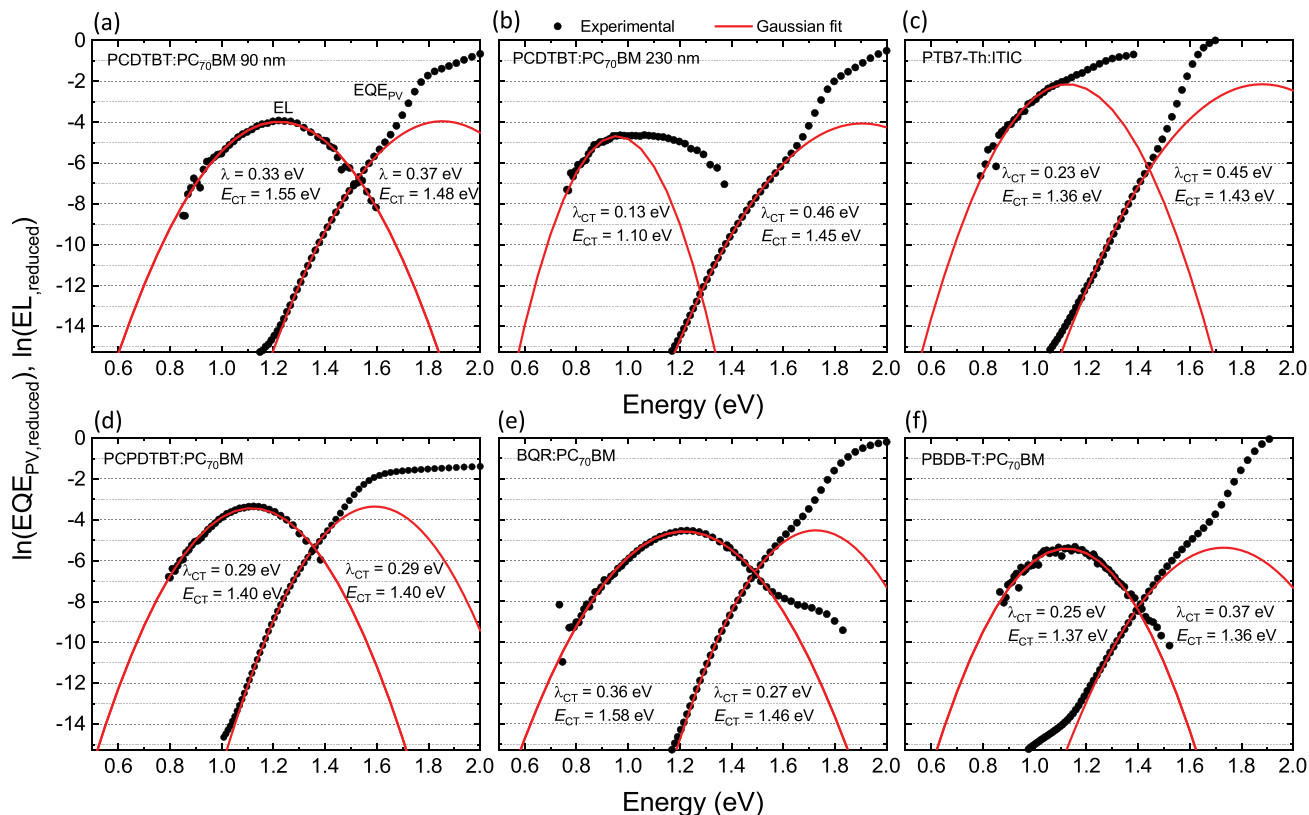


Figure 1. The natural logarithm of the reduced photovoltaic external quantum efficiency (EQE_{PV}) and reduced electroluminescence (EL) for different donor: acceptor pairs. The solid lines are the Gaussian fittings from Equations (1) and (2). The energy of the CT states and reorganization energies obtained from the fittings of EQE_{PV} and EL are separately indicated in each panel.

names and device structures are provided in the Experimental Section. These six combinations include the well-studied PCDTBT:PC₇₀BM system with two different junction thicknesses as well as the non-fullerene PTB7-Th:ITIC. These materials were not “cherry-picked” but were selected such that: (i) the emission is strong enough within the sensitivity range of our photo-multichannel analyzer (300 to 1650 nm); and (ii) the CT state energy be distinguishable from the singlet excitons.

Figure 1 shows the natural logarithms of the reduced EQE_{PV} (i.e., EQE_{PV} multiplied by energy to obtain a Gaussian as per Equation (1)) and reduced EL (i.e., EL divided by energy as per Equation (2)) as a function of energy. The EQE_{PV} spectra were recorded with unprecedented sensitivity using a recently introduced approach^[19] so that in the scale shown in Figure 1 the noise floor corresponds to values below -15 . The dynamic range for the fitting of EQE_{PV} is limited by the exciton absorption (from above) and the sub-gap trap states (from below). The fitting range is thus optimized for the most precise fit. The Gaussian fittings based on Equation (1) are shown on the EQE_{PV} spectra yielding the CT state parameters E_{CT} and λ . The EL spectra were all recorded using the same devices at current densities close to the short circuit current (within a factor 2–3), with a methodology as detailed in the Experimental Section. The Gaussian fittings based upon Equation (2) were applied to EL spectra and the corresponding curves, and the extracted CT parameters are shown in the figure.

The first observation from Figure 1 is that for none of the studied systems do the EQE_{PV} and EL fits result in the same values of the CT parameters although for the thin PCDTBT:PC₇₀BM device the agreement is more acceptable. Furthermore, the CT parameters obtained from PCDTBT:PC₇₀BM devices with different thicknesses (panel a and b) are considerably different. For the 230 nm thick PCDTBT:PC₇₀BM device the reduced EL spectrum substantially deviates from the expected Gaussian shape. For all other systems for both EQE_{PV} and EL, good fittings can be obtained (so that the mathematical uncertainty caused by the fitting error is small), yet the parameters obtained from EQE_{PV} and EL do not agree with each other. These results already provide a hint that the spectra may be influenced by the device optics which depends on the material and the thickness as explained by List et al.^[15] The EQE_{PV} can be partially “reconstructed” from the EL spectra assuming perfect symmetry between EL and EQE_{PV} spectra but such reconstructions are only within the accuracy of semi-logarithmic plots. It is evident here that fitting the EQE_{PV} and EL spectra based on Equations (1)–(4) can result in significantly different CT state parameters.

In order to further probe the potential impact of interference effects on the EQE_{PV} spectra we analyzed PCDTBT:PC₇₀BM devices with multiple different junction thicknesses. This also provided a means to evaluate the absorption pre-factor (f_a) from the absorption coefficient spectra of the CT states.

This pre-factor is required to determine the oscillator strength of the CT states if the number of CT states is known. Accurate determination of the number density of the CT states is challenging (and beyond the scope of this work), so we only determined the pre-factor of the absorption in Equation (3) which is indeed dependent on the number of CT states as well as their absorption cross sections. **Figure 2a** shows the EQE_{PV} spectra of these devices in semi-logarithmic plots and the inset shows them in linear plots. The effect of the cavity optics is obvious from the different spectral shape of the EQE_{PV} spectra in the visible region as shown in the inset. The absorption coefficient spectra were then determined using Equation (4) and are shown in **Figure 2b**. The dotted lines in this plot show the Gaussian fittings based on Equation (4) to determine the CT state parameters. We then used the method of Kaiser et al.^[22] to more accurately obtain the absorption coefficient [i.e., not from Equation (4)] in the sub-gap region from the EQE_{PV} spectra. This “numerically obtained” absorption coefficient is also shown in **Figure 2b** as a bold red dashed line; the respective Gaussian fit is indicated by the red dotted line.

The corresponding measured EL spectra of the same PCDTBT:PC₇₀BM devices are shown in **Figure 2c**. As demonstrated by List et al. the spectral shape of the EL is strongly dependent on the thickness of the device junction. The dashed line indicates the predicted emission spectrum expected for this system based on reciprocity between PL and the numerically obtained absorption coefficient. **Figure 2d** shows example fittings on the measured EL spectra: red-side fitting where a Gaussian is fitted to the lower energy part of the EL peak, and a blue-side fitting where the Gaussian is fitted to the higher energy side of the peak. We note that both such fittings can be found in the literature and while their validity is clearly questionable,^[15] it is therefore instructive to understand and quantify their consequential impact on the absolute errors in the CT state parameterization.

Figure 2e–g shows the results of the EQE_{PV} and EL fits versus active layer thickness using Equations (1) and (2) respectively. The solid horizontal lines indicate the values obtained from fittings using the numerically obtained absorption coefficient α —a thickness independent value. The variations in the parameters with thickness is striking. The error bars indicate the (mathematical) Gaussian fitting error at each thickness which are typically smaller than the absolute error (being the difference between the value obtained from fitting the EQEs and that obtained from the numerically obtained α). As such, these CT state evaluations are precise but not accurate. For example, the reorganization energies obtained from EL fittings (blue side) are subject to absolute errors as large as 250 meV, with EQE_{PV} fittings slightly better with errors of less than 150 meV. The red-side fittings on the EL can vary up to 1 eV (not shown in the scale of **Figure 2e**). For the CT state energies (**Figure 2f**), EQE_{PV} certainly yields a more accurate fit than the EL, with absolute errors less than 50 meV versus extremely large errors on the EL fitting. Finally, **Figure 2g** shows the results of the absorption pre-factor based upon the EQE_{PV} . Depending on the thickness of the active layer, any arbitrary value from 50 to 900 eV²cm⁻¹ can be extracted while that obtained from the numerical α is 450 eV²cm⁻¹. These absolute errors are too large to be neglected even for order-of-magnitude estimations.

While the EL spectra are significantly influenced by the active layer thickness, we should note that the position of the emission zone within the active layer also impacts the emission spectra. The width and position of the emission zone is a complicated function of electron and hole mobility, recombination rate constant, active layer thickness, and the doping level. This effect, being insignificant in thin diodes (≈ 100 nm), becomes pronounced in devices with thicknesses comparable with the half wavelength (see Supporting Information). Again, the asymmetry between the position and width of the EL emission zone and absorption zone (active layer) is a deviation only from the “observed” reciprocity between the EL and the absorption spectrum (i.e., $\approx EQE_{PV}$) and not a deviation from the principle of detailed balance. This discrepancy can be traced back to the different carrier density profiles in the PV and EL modes in such thin film diodes. This is briefly discussed in the Supporting Information, but a more detailed analysis is beyond the scope of this work and will be presented elsewhere.

To further consolidate our experimental findings of the impact of thickness on the spectral shape and magnitude of the CT state contribution to the EQE_{PV} and EL spectra, we conducted electro-optical simulations (details in the Experimental Section). We reconstructed **Figure 2** using the same junction thicknesses. The input parameters to the electro-optical simulations were the complex refractive indices of all active and non-active layers in the device, charge carrier mobilities, and relevant energy levels. Importantly, we note that we used the numerically obtained absorption coefficient from **Figure 2** as an input for the attenuation coefficient (the imaginary part of the complex refractive index) of PCDTBT:PC₇₀BM. Moreover, a Gaussian function was constructed from the EQE_{PV} with the same E_{CT} and λ , and inserted into the EL simulation as the input emission spectrum. We thus imposed reciprocity between the absorption and emission spectra and also stress that these were qualitative simulations; whether the spectra were entirely and intrinsically accurate for PCDTBT:PC₇₀BM plays no role. The aim being to check whether or not the calculated CT state parameters from the simulated EQE_{PV} and EL spectra are in agreement with the assumed input parameters, and if not within what error. The EQE_{PV} spectra were used to determine the absorption pre-factor whilst both EQE_{PV} and EL were fitted to determine E_{CT} and λ . **Figure 3a** shows the electro-optically simulated EQE_{PV} spectra, which are in general agreement with the measured EQE_{PV} s presented in **Figure 2a**. Similar to **Figure 2**, in **Figure 3b** we show the absorption coefficient spectra calculated from the EQE_{PV} s with Gaussian fits (dotted lines) and the dashed line the input spectrum to the simulation. The EL spectra and their blue-side and red-side fittings are shown in **Figure 3c–d** together with the Gaussian fittings based on Equation (2). Finally, fitting results (as per **Figure 2**) are presented in **Figure 3e–g**. In accordance with the fitting results on experimental EQE_{PV} and EL spectra, the results for CT state energy, reorganization energy, and absorption pre-factor for these reconstructed simulations are strongly thickness dependent and different to the values inserted into the simulation as inputs. The input values are shown as solid horizontal lines in **Figure 3e–g**.

The above results, both from experiment and simulation, indicate that the CT state parameterization cannot be simply

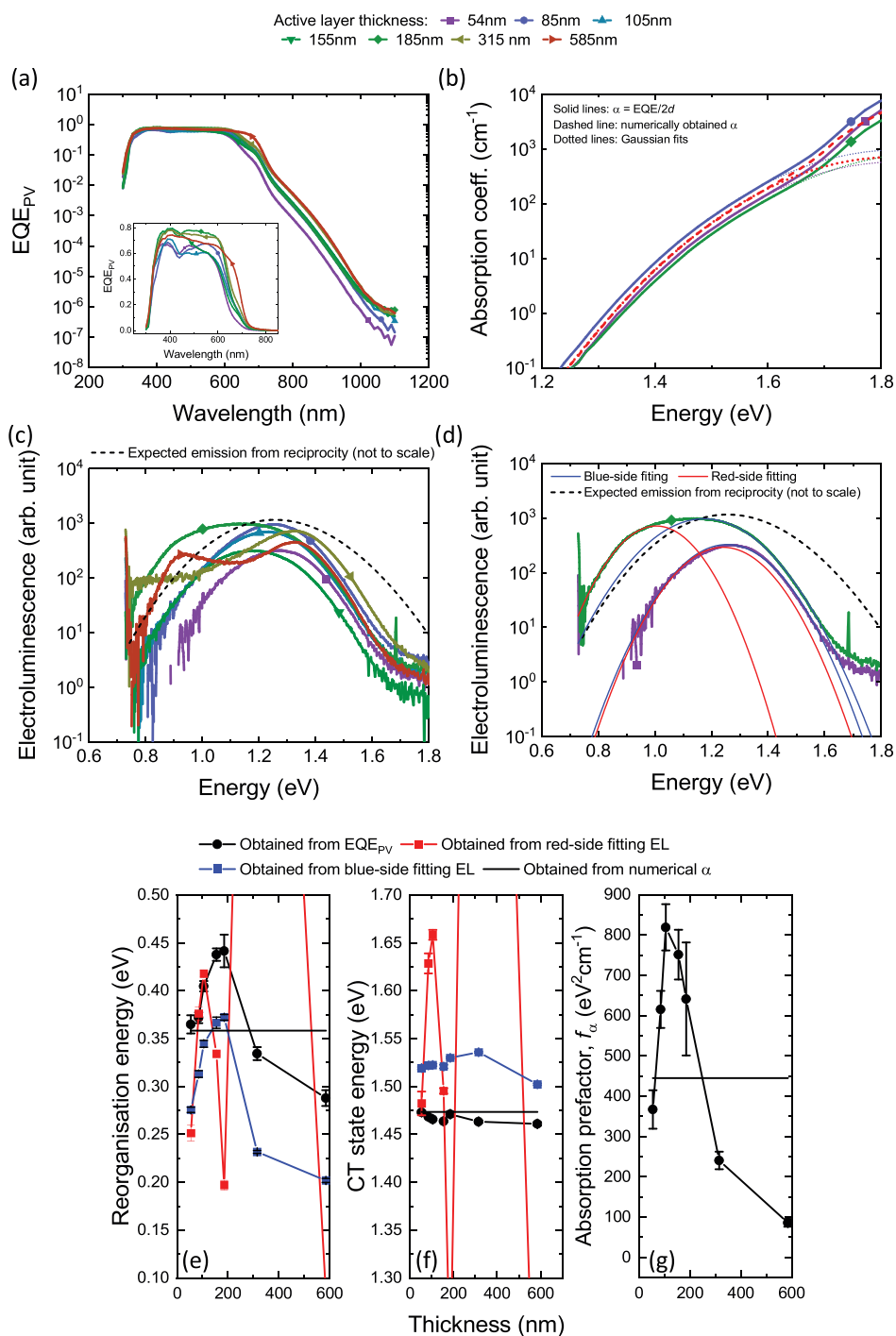


Figure 2. Experimental results of CT state parameterization for PCDTBT:PC₇₀BM solar cells with different thicknesses: a) Semi-logarithmic plot of the EQE_{pV} spectra—the inset shows the linear plot; b) the absorption coefficients versus energy calculated from the EQE_{pV} spectra (selected thicknesses are only shown for better visualization) based on Equation (4) as well as numerically obtained absorption coefficient (the dashed red line). The dotted lines are the Gaussian fits based on Equation (3) to obtain CT parameters; c) EL spectra of the same devices—the dashed black line shows the expected PL spectrum from the CT parameters obtained from fittings on numerical α in panel (b) based on the reciprocity principle; d) Gaussian fittings based on Equation (2) on the emission spectra (selected thicknesses are only shown for better visualization) to obtain CT parameters. Both red-side and blue-side fittings are performed; e–g) the results of Gaussian fittings on the EQE_{pV} and EL spectra as reorganization energy, CT state energy, and absorption pre-factor f_{α} . The error bars indicate the fitting error and the solid horizontal lines are the values obtained from fittings on the numerically obtained α shown as a dashed line in panel (b). The absolute errors are the differences between symbols and the solid horizontal lines.

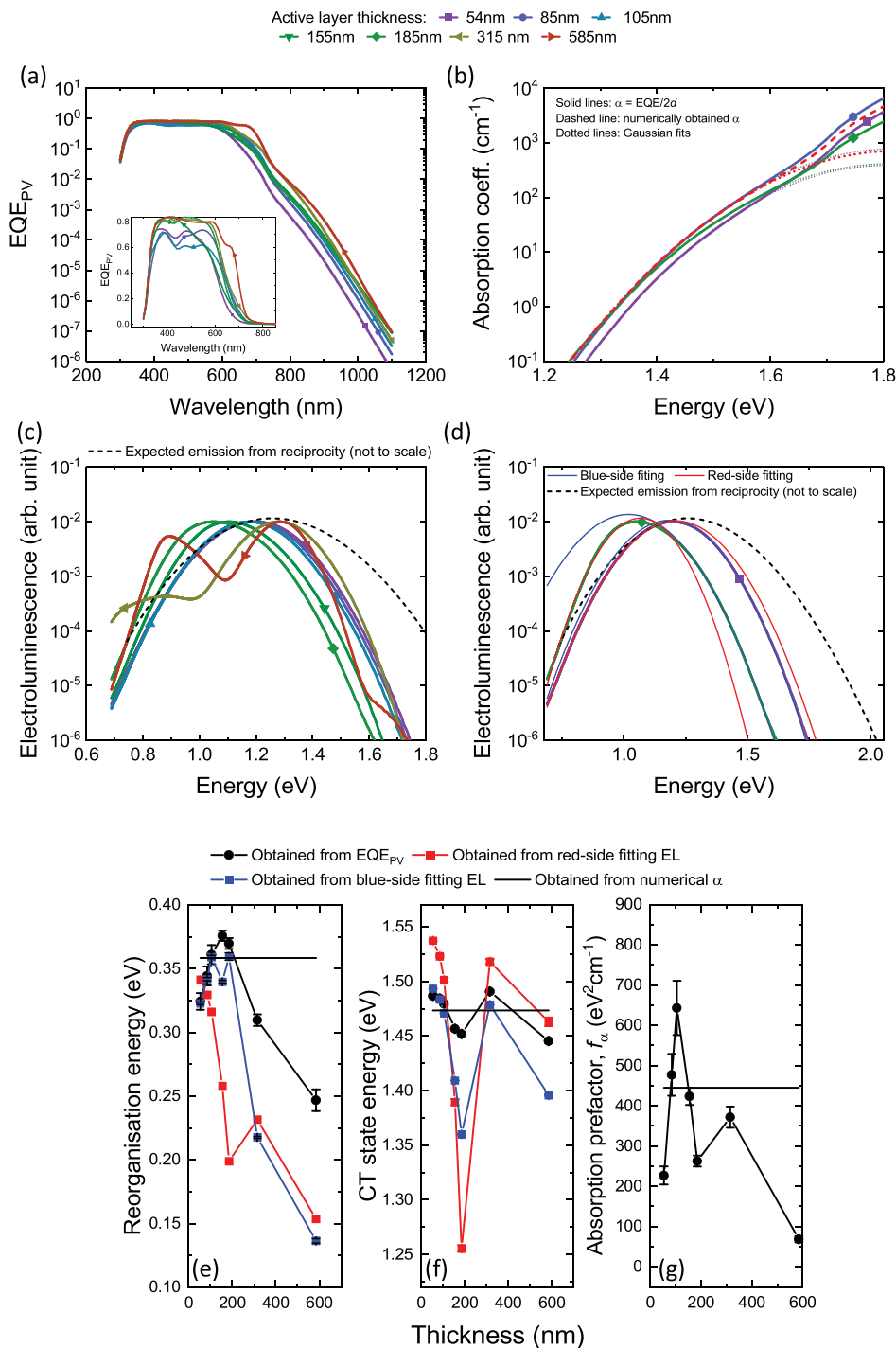


Figure 3. Similar plots as for Figure 2 for PCDTBT:PC₇₀BM devices with different thicknesses but generated using optical and drift and diffusion simulations. All the fittings and analysis are similar to the caption of Figure 2. To obtain the EQE_{PV} spectra, optical constants of the PCDTBT:PC₇₀BM and all other non-active layers were used in a transfer matrix model to predict the absorbance of the active layer. To generate the EL spectra, optical constants were used to calculate the out-coupling and electrical constants of the PCDTBT:PC₇₀BM (electron and hole mobilities and recombination rate constant) were employed in a drift and diffusion program (Fluxim, SETFOS).

extracted using Equation (4). These effects on the EQE_{PV} spectra can be accounted for by considering the cavity, for example by using the methodology explained by Kaiser et al.^[22] The computer code and exemplary data to show this are provided in the

Supporting Information. To extract the CT state parameters from EL spectra, although it may be possible, is more difficult. This is mainly because the effect of the low finesse cavity on the emission is more complex since it is multimodal. The

procedure explained by List et al. provides a correction method for these spectra.^[15] As such the authors suggest the use of EQE_{PV} spectra instead of EL to extract CT state parameters where possible.

The corrected form of Equation (4) relevant for thin film solar cells can be obtained from wave optics (see Supporting Information). EQE_{PV} can then be evaluated as

$$EQE_{PV} = 2d\alpha_{CT} \times f_{int}(E) \quad (5)$$

where $f_{int}(E)$ is a photon energy dependent correction factor due to optical interference or in other words, effectively acting as a passive filter. Accordingly, in the measured EQE_{PV} , the spectral shape of α_{CT} (Equation 3) becomes modified by the function $f_{int}(E)$. The energy dependence of $f_{int}(E)$ is strongly sensitive to the thicknesses and the complex refractive indices of all layers of the device stack and is, therefore, both material and system dependent. This function (see Equation S5, Supporting Information) is derived in the Supporting Information and in the case of perfect reflectance from the back electrode it takes the simple form of

$$f_{int}(E) \approx T(E) \times \left[1 - \frac{hc}{4\pi nEd} \sin\left(\frac{4\pi nE}{hc}d\right) \right] \quad (6)$$

in the limit of weak absorption (e.g., via sub-gap states), corresponding to $\alpha_{CT}d \ll 1$. Here, n is the real part of the complex

refractive index, $hc \approx 1240$ eV·nm, while $T(E)$ is the effective internal intensity transmittance through the layers (influenced by interference effects) in front of the active layer and reflects the solar cell spectral throughput [in-(out)-coupling] function. This function should not be confused with transmittance through the ITO.

Thus, for $\alpha d \ll 1$, the function $f_{int}(E)$ can be viewed as a filter function and its spectral shape must be identical for the emission and absorption due to the reciprocity in linear optics. However, it asymmetrically affects the absorption and emission spectra due to the Stokes shift. Based on the above analysis, the EQE_{PV} can be converted to the absorption coefficient by introducing the oscillatory function $f_{int}(E)$ to Equation (4) [$EQE_{PV} \approx 2d\alpha_{CT}$] that depends on thickness and photon energy. Similarly, for the CT state parameterization based on EQE_{PV} , Equation (5) must be used. The full evaluation of $f_{int}(E)$, including the E dependences of both $T(E)$ and back-electrode reflection [see Equation S5, Supporting Information], is in general analytically intractable and a computer-based transfer matrix approach is therefore needed for this correction. We have used this method to model these functions. This procedure is embedded in the work of Kaiser et al.^[22] to extract the optical constants of sub-gap states from the EQE_{PV} spectra (see Supporting Information for the computer program). **Figure 4** shows the simulated $f_{int}(E)$ (blue solid lines) at different active layer thicknesses, along with the approximate form Equation (6) (red dotted lines) and $T(E)$ (black dashed lines). Indeed, Equation (6) generally reproduces

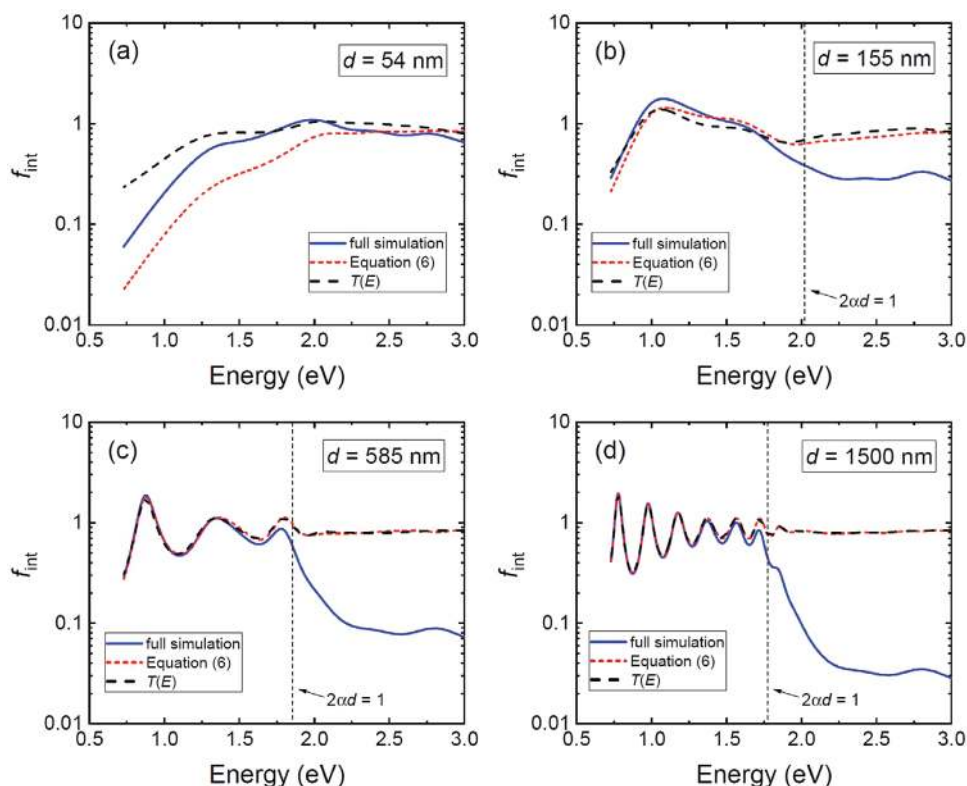


Figure 4. Simulated $f_{int}(E)$ of a PCDTBT:PC₇₀BM solar cell, with active layer thickness of a) 54 nm, b) 155 nm, c) 585 nm, and d) 1500 nm, is indicated by the blue solid line. The approximation Equation (6), assuming weak absorption ($\alpha d \ll 1$) and perfect back-electrode reflection, is indicated by the red dotted line. The calculated $T(E)$ (black dashed lines) are included for comparison.

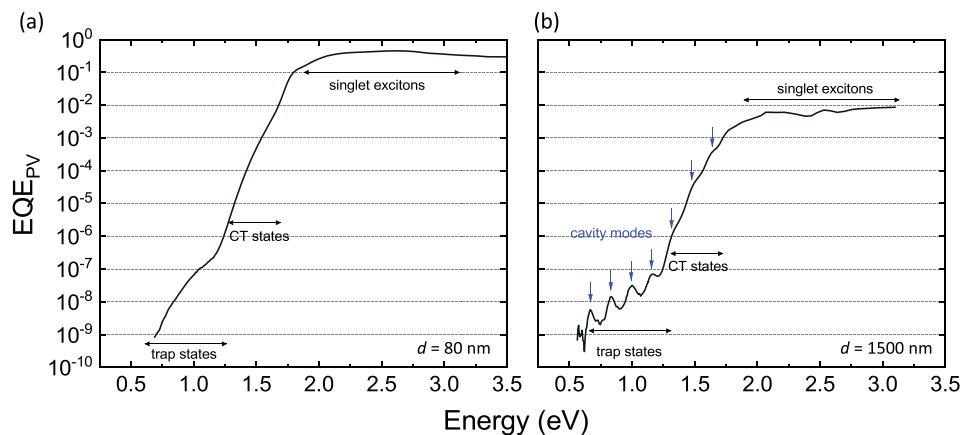


Figure 5. Sensitive EQE_{PV} spectrum of a) a thin PCDTBT:PC₇₀BM device with active layer thickness of 80 nm and b) a thick PCDTBT:PC₇₀BM photo-voltaic device with an active layer thickness of 1500 nm. Three regions are distinguished in the spectra where singlet excitons, CT states, and trap states contribute to the EQE_{PV} . In (b) the cavity modes are shown by the blue arrows appearing as maxima in the EQE.

the oscillatory behavior of $f_{int}(E)$ when $\alpha d \ll 1$, showing good agreement for thicker active layers. In this limit, $f_{int}(E)$ approximately equals $T(E)$ as the second term in the bracket of Equation 6 vanishes with the junction thickness. The oscillatory behavior of $T(E)$ is a result of interference between incoming and reflected optical fields within the optical stack. Note that Equation (6) is not applicable in the strong absorption limit $\alpha d \gg 1$, where we expect all in-coupled light to be absorbed; hence, $EQE_{PV}(E) \approx T(E)$ and therefore, $f_{int}(E) \approx T(E)/(2\alpha d)$.

From Equation (5) it is clear that the EQE_{PV} inherits the oscillatory behavior of $f_{int}(E)$; hence one expects it to also be oscillatory. However, oscillations in the EQE_{PV} spectra are often not observed in devices with standard active layer thicknesses of order of 100s of nm. Such thin active layers form extremely low-finesse cavities with large mode separation and spectrally broad modes as seen from Figure 4 and the slowly varying sine function in Equation (6) when d is small. Therefore, $f_{int}(E)$ does not result in observable and clear peaks in the EQE_{PV} (as shown in Figure 5a for the EQE_{PV} of an 80 nm thick PCDTBT:PC₇₀BM solar cell) but distorts its shape and is the origin of the absolute errors in the CT parameterization shown in Figures 2 and 3. As evident from Figure 4, this scenario changes when the thickness increases and thus the frequency of cavity modes. To unambiguously demonstrate the role of cavity interference in the sub-band gap EQE_{PV} spectral shape, we fabricated an extremely thick PCDTBT:PC₇₀BM device with an active layer thickness of 1500 nm. For this device, a shorter mode separation is expected in accordance with Figure 4. Figure 5b shows the sensitive EQE_{PV} of this thick PCDTBT:PC₇₀BM device versus photon energy. Cavity modes are clearly manifest as evenly separated peaks in the EQE_{PV} spectrum. The CT state band expands from 1.2 to 1.8 eV with 3 clear cavity oscillations superimposed upon it. From 0.5 to 1.2 eV the contribution of trap states is notable which is again superimposed with 4 cavity modes appearing as maxima. These maxima indeed are not observable above the gap where the material is strongly absorbing and the cavity modes are damped out.

Finally, it should be stressed that the applicability of the presented CT state parameterization is subject to sufficient spectral separation between CT state absorption/emission and the

singlet excitons. This deconvolution is particularly problematic for so-called low-offset systems^[23,24] such as the NFAs currently showing the highest power conversion efficiencies^[25,26] where the CT state and exciton features are almost degenerate.^[27–29] In this limit, the CT parameterization via non-adiabatic Marcus theory irrespective of cavity optics is inappropriate, as exemplified for two high efficiency NFA systems PM6:Y6 and PM6:ITIC in the Supporting Information. As more high efficiency, low-offset (NFA) systems are reported, this CT state parameterization issue will become more prominent—and we would contend that the electro-optical principle and methods derived over many years for the fullerenes cannot simply be translated to the NFAs.

3. Conclusions

Parameterization of the CT states of acceptor: donor organic semiconducting combinations based upon Gaussian fittings to sub-gap absorption or EQE_{PV} and EL spectra has become a standard tool in organic solar cells. We have shown that CT state parameterization can result in totally arbitrary values due to the often-ignored cavity effects. By studying a number of archetypal and emerging acceptor: donor systems, we have shown that, to varying extents, the measured EQE_{PV} or EL spectra on which the fittings are performed are subject to low finesse cavity interference that cannot be neglected. Interference effects can be accounted for by determining a thickness independent “numerically obtained absorption coefficient” form EQE_{PV} using the inverse transfer matrix approach of Kaiser et al.^[22] If the CT state and singlet exciton absorptions are sufficiently distinguishable from each other, this allows a more a rational CT state parameterization from EQE_{PV} . EL spectra are more adversely affected by the interference effects, and simple plane wave transfer matrix approaches are not adequate to fully account for their impact. We demonstrate the magnitude of the relative errors for the PCDTBT:PC₇₀BM system as a function of junction thickness. In particular, the results clearly show that the Beer–Lambert assumption for sub-gap absorption is invalid producing relative errors as large as

90% in the absorption cross section of the CT states. We also provide an analytical framework to convert the EQE_{PV} to an absorption coefficient by introducing an oscillatory function f_{int} (the effective spectral throughput of the cavity) that depends on thickness and photon energy—this can be used in combination with transfer matrix analysis to enhance the accuracy of the CT state parameterization. Finally, we note that so called low-offset systems such as the new high efficiency non-fullerene acceptors pose particular challenges for CT state parameterization. It appears the only way forward for these systems is to reconstruct “interference-free” thickness-independent emission spectra. This is not a trivial task because of the complex multimodal nature of the wave optics of light emission in a low-Q cavity. We would stress that these findings in no way challenge the fundamental validity of reciprocity and the thermodynamics of solar cells. They merely highlight the asymmetric nature of emission and absorption mode coupling in thin film optoelectronic cavities.

4. Experimental Section

Materials: PCDTBT (Poly[N-9'-heptadecanyl-2,7-carbazole-alt-5,5-(4',7'-di-2-thienyl-2',1',3'-benzothiadiazole)]) and PCPDTBT (Poly[2,6-(4,4-bis-(2-ethylhexyl)-4H-cyclopenta[2,1-b;3,4-b']-dithiophene)-alt-4,7-(2,1,3-benzothiadiazole)]) were purchased from Sigma Aldrich. PTB7-Th (Poly[4,8-bis(5-(2-ethylhexyl)thiophen-2-yl)benzo[1,2-b;4,5-b']dithiophene-2,6-diyl-alt-(4-(2-ethylhexyl)-3-fluorothieno[3,4-b]thiophene)-2-carboxylate-2,6-diyl)], ITIC (3,9-bis(2-methylene-(3-(1,1-dicyanomethylene)-indanone))-5,5,11,11-tetrakis(4-hexylphenyl)-dithieno[2,3-d:2',3'-d']-s-indaceno[1,2-b:5,6-b']dithiophene), PBDB-T (Poly[(2,6-(4,8-bis(5-(2-ethylhexyl)thiophen-2-yl)-benzo[1,2-b:4,5-b']dithiophene))-alt-(5,5-(1',3'-di-2-thienyl-5',7'-bis(2-ethylhexyl)benzo[1',2'-c:4',5'-c']dithiophene-4,8-dione))], PM6 (Poly[(2,6-(4,8-bis(5-(2-ethylhexyl)-3-fluoro)thiophen-2-yl)-benzo[1,2-b:4,5-b']dithiophene))-alt-(5,5-(1',3'-di-2-thienyl-5',7'-bis(2-ethylhexyl)benzo[1',2'-c:4',5'-c']dithiophene-4,8-dione))], and Y6 (2,2'-(2Z,2'Z)-((12,13-bis(2-ethylhexyl)-3,9-diundecyl-12,13-dihydro-[1,2,5]thiadiazolo[3,4-e]thieno[2'',3''':4',5']thieno[2',3':4,5]pyrrolo[3,2-g]thieno[2',3':4,5]thieno[3,2-b]indole-2,10-diyl)bis(methanylylidene)bis(5,6-difluoro-3-oxo-2,3-dihydro-1H-indene-2,1-diylidene)dimalononitrile) were purchased from Zhi-yan (Nanjing) Inc. PC₇₀BM ((6,6)-phenyl-C71-butyric acid methyl ester) was purchased from Solarmer, and BQR (benzodithiophene-quaterthiophene-rhodanine) was received from Dr. David. J Jones (University of Melbourne).

Device Fabrication: PCDTBT:PC₇₀BM devices were fabricated in a conventional structure (ITO/PEDOT:PSS/PCDTBT:PC₇₀BM/PDINO/Al) with the following procedures: 30 nm PEDOT:PSS films were spin-coated (5000 rpm) on pre-cleaned ITO substrate and further annealed at 155 °C for 10 min. Then PCDTBT:PC₇₀BM (with weight ratio of 1:4) films with different thicknesses were cast onto the PEDOT:PSS coated substrates from 1,2-dichlorobenzene solution with different spin-coating speeds (30 mg mL⁻¹ solution with 1500 rpm for 54 nm active layer, 40 mg mL⁻¹ solution with 1500 rpm for 85 nm active layer, 40 mg mL⁻¹ solution with 1000 rpm for 105 nm active layer, 40 mg mL⁻¹ solution with 600 rpm for 155 nm active layer, 50 mg mL⁻¹ solution with 600 rpm for 185 nm active layer, 60 mg mL⁻¹ solution with 600 rpm for 315 nm active layer, and 60 mg mL⁻¹ solution with 400 rpm for 585 nm active layer). Afterward, an ≈8 nm thick PDINO film was spin-coated (3000 rpm) onto the PCDTBT:PC₇₀BM films from methanol solution (1 mg mL⁻¹), and 100 nm aluminium was then thermally evaporated (at a pressure of 10⁻⁷ mbar) as the cathode. The BQR:PC₇₀BM devices were fabricated in a conventional structure (ITO/PEDOT:PSS/BQR:PC₇₀BM/Ca/Al) with the following procedures: 30 nm PEDOT:PSS film was deposited as described above, and then 100 nm BQR:PC₇₀BM (1:1, w/w) films were

spin-coated (1000 rpm) on PEDOT:PSS film from toluene (24 mg mL⁻¹), and further treated with solvent annealing (toluene) for 20 s and thermal annealing at 90 °C for 10 min. Devices were then completed by thermally evaporating 10 nm Ca and 100 nm Al as the cathode. PCPDTBT:PC₇₀BM, PTB7-Th:ITIC, PBDB-T:PC₇₀BM, PM6:ITIC, and PM6:Y6 devices were fabricated in inverted structures (ITO/ZnO/Active layer/MoO₃/Ag). In all these inverted devices, a 30 nm solution processed ZnO film acted as the electron transport layer and was fabricated with the following procedures: ZnO solution was first prepared by dissolving zinc acetate dihydrate (200 mg) in 2-methoxyethanol (2 mL) and ethanolamine (56 μL) and further stirred overnight under ambient conditions. Then ZnO solution was spin-coated (3000 rpm) onto ITO substrates and thermally annealed at 200 °C for 60 min. The active layers of those above systems were deposited on ZnO the films with the following method: (1) For PCPDTBT:PC₇₀BM devices, 80 nm PCPDTBT:PC₇₀BM (1:4, w/w) film was spin-coated (1500 rpm) from 1,2-dichlorobenzene solution (40 mg mL⁻¹) with no further treatment; (2) For PTB7-Th:ITIC devices, 100 nm PTB7-Th:ITIC (1:1.4, w/w) film was spin-coated (1000 rpm) from chlorobenzene (14 mg mL⁻¹ with 1 vol% DIO) solution with no further treatment; (3) For PBDB-T:PC₇₀BM devices, 100 nm PBDB-T:PC₇₀BM (1:1, w/w) film was spin-coated (1000 rpm) from chlorobenzene (14 mg mL⁻¹ with 3 vol% DIO) solution and further rinsed with 80 μL of methanol at 4000 rpm for 20 s to remove the residual DIO; (4) For PM6:ITIC devices, 100 nm PM6:ITIC (1:1, w/w) film was spin-coated (1000 rpm) from chlorobenzene solution (18 mg mL⁻¹ with 0.5 vol.% DIO) and annealed at 100 °C for 10 min; (5) For PM6:Y6 devices, 100 nm PM6:Y6 film (1:1.2, w/w) was spin-coated (3000 rpm) from chloroform solution (16 mg mL⁻¹ with 0.5 vol.% 1-chloronaphthalene) and further annealed at 110 °C for 10 min. After depositing all of these active layers, 7 nm MoO₃ and 100 nm Ag were thermally evaporated as the anode.

Photovoltaic External Quantum Efficiency Measurements: For sensitive measurements of the EQE_{PV} , a Lambda 950 spectrophotometer (PerkinElmer) was used as a light source. The output light from the monochromator was physically chopped at 273 Hz (Thorlabs MC2000B) and different OD4 long-pass filters (Edmunds Optics) were used to filter out remaining parasitic stray light. Prior to detecting the photocurrent with a lock-in amplifier (Stanford Research System, SR860) using the chopper as an external reference source, the signal was passed through a current pre-amplifier (Femto, DLPCA-200). For calibration, a Newport NIST-calibrated silicon 818-UV, germanium 818-IR and Thorlabs indium gallium arsenide S148C photodiode sensors were used. A detailed experimental description of the sensitive EQE_{PV} measurement is provided in the citation.^[19]

Electroluminescent Measurements: For this measurement, the devices were driven by constant currents applied by a Keithley (2400) source meter unit. Two photonic multi-channel analyzers, PMA 12 and C10028 (HAMAMATSU), with different spectral range (from 346 to 1100 nm and from 896 to 1688 nm, respectively) were used to detect the EL spectra.

Supporting Information

Supporting Information is available from the Wiley Online Library or from the author.

Acknowledgements

The authors thank Dr David Jones of Melbourne University for providing BQR. The work was supported by the Sêr Cymru II Program through the European Regional Development Fund, Welsh European Funding Office, and Swansea University strategic initiative in Sustainable Advanced Materials. A.A. is a Sêr Cymru II Rising Star Fellow and P.M. is a Sêr Cymru II National Research Chair. S.Z. and C.K. are recipients of EPSRC Doctoral Training Partnership studentships.

Conflict of Interest

The authors declare no conflict of interest.

Keywords

charge transfer states, electroluminescence, external quantum efficiency, organic photovoltaics, reciprocity principle

Received: June 3, 2020

Revised: August 24, 2020

Published online:

-
- [1] T. M. Clarke, J. R. Durrant, *Chem. Rev.* **2010**, *110*, 6736.
- [2] K. Vandewal, S. Albrecht, E. T. Hoke, K. R. Graham, J. Widmer, J. D. Douglas, M. Schubert, W. R. Mateker, J. T. Bloking, G. F. Burkhard, *Nat. Mater.* **2014**, *13*, 63.
- [3] K. Vandewal, K. Tvingstedt, A. Gadisa, O. Inganäs, J. V. Manca, *Nat. Mater.* **2009**, *8*, 904.
- [4] S. M. Menke, A. Sadhanala, M. Nikolka, N. A. Ran, M. K. Ravva, S. Abdel-Azeim, H. L. Stern, M. Wang, H. Sirringhaus, T.-Q. Nguyen, *ACS Nano* **2016**, *10*, 10736.
- [5] S. Shoaee, A. Armin, M. Stolterfoht, S. M. Hosseini, J. Kurpiers, D. Neher, *Sol. RRL* **2019**, *3*, 1900184.
- [6] C. Deibel, T. Strobel, V. Dyakonov, *Adv. Mater.* **2010**, *22*, 4097.
- [7] K. Vandewal, K. Tvingstedt, A. Gadisa, O. Inganäs, J. V. Manca, *Phys. Rev. B* **2010**, *81*, 125204.
- [8] J. Benduhn, K. Tvingstedt, F. Piersimoni, S. Ullbrich, Y. Fan, M. Tropicano, K. A. McGarry, O. Zeika, M. K. Riede, C. J. Douglas, *Nat. Energy* **2017**, *2*, 17053.
- [9] R. E. Willems, C. H. Weijtens, X. de Vries, R. Coehoorn, R. A. Janssen, *Adv. Energy Mater.* **2019**, *9*, 1803677.
- [10] T. Kirchartz, J. Nelson, U. Rau, *Phys. Rev. Appl.* **2016**, *5*, 054003.
- [11] A. Melianas, N. Felekidis, Y. Puttison, S. C. Meskers, O. Inganäs, W. M. Chen, M. Kemerink, *Proc. Natl. Acad. Sci. USA* **2019**, *116*, 23416.
- [12] C. Kaiser, K. S. Schellhammer, J. Benduhn, B. Siegmund, M. Tropicano, J. Kublitski, D. Spoltore, M. Panhans, O. Zeika, F. Ortmann, *Chem. Mater.* **2019**, *31*, 9325.
- [13] I. R. Gould, D. Noukakis, L. Gomez-Jahn, R. H. Young, J. L. Goodman, S. Farid, *Chem. Phys.* **1993**, *176*, 439.
- [14] D. C. Coffey, B. W. Larson, A. W. Hains, J. B. Whitaker, N. Kopidakis, O. V. Boltalina, S. H. Strauss, G. Rumbles, *J. Phys. Chem. C* **2012**, *116*, 8916.
- [15] M. List, T. Sarkar, P. Perkhun, J. Ackermann, C. Luo, U. Würfel, *Nat. Commun.* **2018**, *9*, 3631.
- [16] O. Ambacher, W. Rieger, P. Ansmann, H. Angerer, T. Moustakas, M. Stutzmann, *Solid State Commun.* **1996**, *97*, 365.
- [17] T. Gotoh, S. Nonomura, S. Hirata, S. Nitta, *Appl. Surf. Sci.* **1997**, *113*, 278.
- [18] K. Vandewal, L. Goris, I. Haeldermans, M. Nesládek, K. Haenen, P. Wagner, J. Manca, *Thin Solid Films* **2008**, *516*, 7135.
- [19] S. Zeiske, C. Kaiser, P. Meredith, A. Armin, *ACS Photonics* **2019**, *7*, 256.
- [20] A. Armin, M. Velusamy, P. Wolfer, Y. Zhang, P. L. Burn, P. Meredith, A. Pivrikas, *ACS Photonics* **2014**, *1*, 173.
- [21] G. F. Burkhard, E. T. Hoke, M. D. McGehee, *Adv. Mater.* **2010**, *22*, 3293.
- [22] C. Kaiser, S. Zeiske, P. Meredith, A. Armin, *Adv. Opt. Mater.* **2020**, *8*, 1901542.
- [23] S. M. Menke, N. A. Ran, G. C. Bazan, R. H. Friend, *Joule* **2018**, *2*, 25.
- [24] F. D. Eisner, M. Azzouzi, Z. Fei, X. Hou, T. D. Anthopoulos, T. J. S. Dennis, M. Heeney, J. Nelson, *J. Am. Chem. Soc.* **2019**, *141*, 6362.
- [25] L. Meng, Y. Zhang, X. Wan, C. Li, X. Zhang, Y. Wang, X. Ke, Z. Xiao, L. Ding, R. Xia, *Science* **2018**, *361*, 1094.
- [26] J. Yuan, Y. Zhang, L. Zhou, G. Zhang, H.-L. Yip, T.-K. Lau, X. Lu, C. Zhu, H. Peng, P. A. Johnson, *Joule* **2019**, *3*, 1140.
- [27] J. Hou, O. Inganäs, R. H. Friend, F. Gao, *Nat. Mater.* **2018**, *17*, 119.
- [28] L. Perdígón-Toro, H. Zhang, A. Markina, J. Yuan, S. M. Hosseini, C. M. Wolff, G. Zuo, M. Stolterfoht, Y. Zou, F. Gao, *Adv. Mater.* **2020**, *32*, 1906763.
- [29] A. Karki, J. Vollbrecht, A. L. Dixon, N. Schopp, M. Schrock, G. M. Reddy, T. Q. Nguyen, *Adv. Mater.* **2019**, *31*, 1903868.